

NONLINEAR DEFORMATION OF Au, AuSi AND AuCuSi WITH FCC STRUCTURE UNDER PRESSURE

Nguyen Quang Hoc¹ and Nguyen Duc Hien²

¹*Faculty of Physics, Hanoi National of Education University*

²*Mac Dinh Chi High School, Chu Pah District, Gia Lai province*

Abstract. On the basis of the model and the theory of nonlinear deformation for FCC substitutional and interstitial ternary alloy built by the statistical moment method, we perform numerical calculations for Au, AuSi, and AuCuSi. Some calculated results on the nonlinear deformation of Au obtained by SMM have been compared with the experimental data and have some very good concordance. Many calculated numerical results on nonlinear deformation of AuSi and AuCuSi are new and predictive, experimentally oriented

Keywords: substitutional and interstitial ternary alloy, deformation energy density, real stress, elastic deformation limit, statistical moment method.

1. Introduction

Metal Au and interstitial alloys AuSi, AuCuSi have many unusual physical properties and functional important applications. Gold silicide is one of the numerous metal alloys with the trade name AE AlloysTM. They are available as ingot, ribbon, bar, shot, wire, foil, and sheet. Ultra-high-purity and high-purity forms also include metal powder, micron powder, nanoscale, pellets for chemical vapor deposition (CVD), and targets for thin film deposition and physical vapor deposition (PVD) applications. Custom and typical packaging are available. Primary applications include bearing assembly, casting, ballast, radiation shielding, and step soldering.

The dependence of elastic and nonlinear deformations of materials on temperature and pressure has a very important role in predicting and understanding their interatomic interactions, strength, mechanical stability, phase transition mechanisms, and dynamical response. Theoretical and experimental results on the nonlinear and elastic deformation of gold and its interstitial alloys are given in [1-6]. The experimental data on the nonlinear deformation of pure gold are presented in [1-4]. Numerical calculations for many metals

Received May 27, 2022. Revised June 4, 2022. Accepted June 28, 2022.

Contact Nguyen Quang Hoc, e-mail address: hocnq@hnue.edu.vn

are compared with *ab initio* calculations and experiments [5]. Deformation mechanisms in the mechanical response of nanoporous gold are investigated by molecular dynamics simulations [6]

We applied the statistical moment method (SMM) [7] to study many thermomechanical properties of metals and alloys [8-17]. The elastic and thermodynamic properties of inert gas crystals and metals are studied in [8, 9]. We have studied the thermodynamic and melting properties, the elastic deformation for body-centered cubic (BCC) and face-centered cubic (FCC) ternary and binary interstitial alloys [10-15], the melting property for BCC binary substitutional alloys [16], and the theory of nonlinear deformation for BCC and FCC ternary interstitial alloys [17] under pressure.

In this paper, we present a model of alloy, steps of calculating nonlinear deformation quantities for FCC substitutional and interstitial ternary alloy and carry out numerical calculations for Au, AuSi, and AuCuSi.

2. Content

2.1. Model and calculation method

In our model for FCC interstitial alloy AC with condition $c_C \ll c_A$, ($c_X = \frac{N_X}{N}$ ($X = A, C$) is the concentration of atoms X, N_X is the number of atoms X, $N = N_A + N_C$ is the total number of atoms of the alloy AC), the interstitial atom C stays in the body center, the main metal atom A_1 stays in face center and the main metal atom A_2 stays in vertice of cubic unit cell [13, 15].

In our model for FCC interstitial and substitutional alloy ABC with condition $c_C \ll c_B \ll c_A$, the interstitial atom C stays in the body center, the substitutional metal atom B stays in the face center and the main metal atom A_2 stays in the vertice of cubic unit cell [17].

We proceed with numerical calculations of nonlinear deformation quantities of FCC interstitial and substitutional alloy ABC in the following steps:

1-Determine the nearest neighbor distance $r_{1X}(P,0)$ ($X = A, A_1, A_2, C$) between two atoms A in pure metal A and between atom A_1 or A_2 or C and another atom in interstitial alloy AC at pressure P and temperature $T = 0$ K from the equation of state as follows [7, 17].

$$Pv_X = -r_{1X} \left(\frac{1}{6} \frac{\partial u_{0X}}{\partial r_{1X}} + \frac{\hbar \omega_{0X}}{4k_X} \frac{\partial k_X}{\partial r_{1X}} \right) \quad (1)$$

where $v_X = \frac{r_{1X}^3}{\sqrt{2}}$ is the volume of the cubic unit cell corresponding to an atom X of the FCC lattice, u_{0X} is the cohesive energy for atom X, k_X is the harmonic crystal parameter for atom X, $\omega_{0X} = \sqrt{\frac{k_X(P,0)}{m_X}}$ is the vibrational frequency of atom X, at pressure P and temperature $T = 0$ K, m_X is the mass of atom X and $\hbar = \frac{h}{2\pi}$, h is the Planck constant.

2-Determine the harmonic crystal parameter $k_X(P,0)$ and anharmonic crystal parameters $\gamma_{1X}(P,0)$, $\gamma_{2X}(P,0)$, $\gamma_X(P,0)$ of atom X at pressure P and temperature $T = 0$ K according to formulas in [7, 17].

3-Determine the displacement $y_X(P,T)$ of atom X at pressure P and temperature T from the equilibrium position according to formulas in [7, 17].

4-Determine the nearest neighbor distance $r_{1X}(P,T)$ according to the following formulas [7, 17].

$$\begin{aligned} r_{1C}(P,T) &= r_{1C}(P,0) + y_A(P,T), r_{1A}(P,T) = r_{1A}(P,0) + y_A(P,T), \\ r_{1A_1}(P,T) &= r_{1C}(P,T), r_{1A_2}(P,T) = r_{1A_2}(P,0) + y_C(P,T). \end{aligned} \quad (2)$$

5-Determine the mean nearest neighbor distance $\overline{r_{1A}^{AC}(P,T)}$ between two atoms A in alloy AC at pressure P and temperature T according to the following formula [7, 17].

$$\overline{r_{1A}^{AC}(P,T)} = \overline{r_{1A}^{AC}(P,0) + y(P,T)}, \overline{r_{1A}^{AC}(P,0)} = (1 - c_C) r_{1A}(P,0) + c_C r'_{1A}(P,0), \overline{y(P,T)} = \sum_X c_X y_X(P,T), \quad (3)$$

where $r'_{1A}(P,0) = \sqrt{2} r_{1C}(P,0)$, $c_A = 1 - 15c_C$, $c_{A_1} = 6c_C$, $c_{A_2} = 8c_C$ for FCC lattice, $\overline{r_{1A}^{AC}(P,0)}$ is the mean nearest neighbor distance between two atoms A in alloy AC at pressure P and temperature $T = 0$ K, $\overline{y(P,T)}$ is the mean displacement of atom A at pressure P and temperature T from the equilibrium position, $r_{1A}(P,0)$ is the nearest neighbor distance between two atoms A in pure metal A at pressure P and temperature $T = 0$ K and $r'_{1A}(P,0)$ is nearest neighbor distance between two atoms A in the region containing the interstitial atom C at pressure P and temperature $T = 0$ K.

6-Determine the mean nearest neighbor distance a_{ABC} between two atoms A in alloy ABC at pressure P and temperature T according to the formula [7, 17].

$$\begin{aligned} a_{ABC} &= c_{AC} a_{AC} \frac{B_{TAC}}{B_T} + c_B r_{1B} \frac{B_{TB}}{B_T}, \quad \overline{B_T} = c_{AC} B_{TAC} + c_B B_{TB}, c_{AC} = c_A + c_C, a_{AC} \equiv \overline{r_{1A}(P,T)}, \\ B_{TAC} &= \frac{1}{\chi_{TAC}}, \quad \chi_{TAC} = \frac{3 \left(\frac{a_{AC}}{a_{0AC}} \right)^3}{2P + \frac{a_{AC}^2}{3V_{AC}} \left(\frac{\partial^2 \Psi_{AC}}{\partial a_{AC}^2} \right)_T}, B_{TB} = \frac{1}{\chi_{TB}}, \quad \chi_{TB} = \frac{3 \left(\frac{r_{1B}}{r_{0B}} \right)^3}{2P + \frac{r_{1B}^2}{3v_B} \left(\frac{\partial^2 \psi_B}{\partial r_{1B}^2} \right)_T}, \\ \left(\frac{\partial^2 \Psi_{AC}}{\partial a_{AC}^2} \right)_T &\approx N \sum_X c_X \left(\frac{\partial^2 \psi_X}{\partial r_{1X}^2} \right)_T, \end{aligned} \quad (4)$$

where the cohesive energy and crystal parameters for atom B are determined analogically as for atom X, ψ_X, ψ_B respectively are the Helmholtz free energies per an atom X and per an atom B [7, 17], $\Psi_{AC} = N \sum_X c_X \psi_X - TS_c^{AC}$ ($X = A, A_1, A_2, C$) is the Helmholtz free energy of alloy AC, S_c^{AC} is the configurational entropy of alloy AC.

7-Determine the Helmholtz free energy of alloy ABC at pressure P and temperature T according to the formula [7, 17].

$$\Psi_{ABC} = \Psi_{AC} + Nc_B(\psi_B - \psi_A) + TS_c^{AC} - TS_c^{ABC},$$

where S_c^{ABC} is the configurational entropy of alloy ABC.

8-Determine the Young modulus of alloy ABC according to the formula [7, 17].

$$E_{YABC} = E_{YAC} + c_B(E_{YA} - E_{YB}), E_{YAC} = E_{YA} \frac{\sum_X c_X \frac{\partial^2 \psi_X}{\partial \varepsilon^2}}{\frac{\partial^2 \psi_A}{\partial \varepsilon^2}},$$

$$E_{YM} = \frac{1}{\pi \cdot r_{1M} A_{1M}}, A_{1M} = \frac{1}{k_M} \left[1 + \frac{2\gamma_M^2 \theta^2}{k_M^4} \left(1 + \frac{1}{2} Y_M \right) (1 + Y_M) \right]. \quad (5)$$

Here, $\theta = k_{Bo} T, k_{Bo}$ is the Boltzmann constant.

9-Determine the mean nearest neighbor distance $\overline{r_{1A}^{ACF}}(P, T)$ between two atoms A in alloy AC, the mean nearest neighbor distance $a_{ABC}^F(P, T)$ between two atoms A in alloy AC, and the Helmholtz free energy $\Psi_{ABC}^F(P, T)$ at pressure P and temperature T after deformation according to the formulas in [7, 17].

10-Determine the density of deformation energy $f_{ABC}(\varepsilon)$ according to formula [7, 17].

$$f_{ABC}(\varepsilon) = \sum_X c_X \left\{ \psi_X \left(\frac{1}{v_{ABC}^F} - \frac{1}{v_{ABC}} \right) + \frac{2\varepsilon r_{01X}^F}{v_{ABC}^F} \left(\frac{\partial \psi_X^F}{\partial r_{1X}^F} \right)_T + \frac{\varepsilon^2}{2v_{ABC}^F} \left[\left(\frac{\partial^2 \psi_X^F}{\partial r_{1X}^{F2}} \right)_T (2r_{01X}^F)^2 + \right. \right.$$

$$\left. \left. + \left(\frac{\partial \psi_X^F}{\partial r_{1X}^F} \right)_T 2r_{01X} \right] \right\} - c_B \left\{ \psi_A \left(\frac{1}{v_{ABC}^F} - \frac{1}{v_{ABC}} \right) + \frac{2\varepsilon r_{01A}^F}{v_{ABC}^F} \left(\frac{\partial \psi_A^F}{\partial r_{1A}^F} \right)_T + \right.$$

$$\left. \left. + \frac{\varepsilon^2}{2v_{ABC}^F} \left[\left(\frac{\partial^2 \psi_A^F}{\partial r_{1A}^{F2}} \right)_T (2r_{01A}^F)^2 + \left(\frac{\partial \psi_A^F}{\partial r_{1A}^F} \right)_T 2r_{01A} \right] \right\}, X_1 = A, A_1, A_2, B, C, \quad (6)$$

where ε is the strain.

11-Determine the strain ε^F corresponding to the maximum value of density of deformation energy $f_{ABC \max}$.

12-Determine the maximum real stress $\sigma_{1 \max}$ according to the formula [7, 17].

$$\sigma_{1 \max} = \frac{f_{ABC \max}}{C_{ABC} \varepsilon^F (1 + \varepsilon^F)}, \quad (7)$$

where $C_{ABC} = \frac{f_{ABC}(\varepsilon_{0.2})}{\sigma_{0.2}\varepsilon_{0.2}}$ with $\sigma_{0.2}, \varepsilon_{0.2}$ are the experimental values of the stress and the strain of the alloy ABC at $\varepsilon = 0.2\%$.

13-Determine the limit of elastic deformation σ_e according to formula [7, 17].

$$\sigma_e = E_{ABC}\varepsilon_e = \sigma_{0ABC} \frac{\varepsilon_e^{\alpha_{ABC}}}{1 + \varepsilon_e}. \quad (8)$$

Here, ε_e is the strain corresponding to the limit of elastic deformation σ_e , the constants σ_{0ABC} and α_{ABC} have different values for different alloys ABC.

14-When the substitutional atom concentration is zero, we obtain the nonlinear deformation quantities of the interstitial alloy AC.

15-When the substitutional atom concentration and the interstitial atom concentration are zero, we obtain the nonlinear deformation quantities of the main metal A.

We perform numerical calculations according to above mentioned steps for Au, AuSi, and AuCuSi in subsection 2.2.

2.2. Numerical results and discussions for Au, AuSi, and AuCuSi

For interactions Au-Au, Cu-Cu, Si-Si in Au, AuSi, and AuCuSi, we use the Mie-Lennard-Jones potential [18, 19].

$$\varphi(r) = \frac{D}{n-m} \left[m \left(\frac{r_0}{r} \right)^n - n \left(\frac{r_0}{r} \right)^m \right], \quad (9)$$

where D is the depth of potential well corresponding to the equilibrium distance r_0 , m and n are determined empirically. In our model of ternary alloy, we do not use the interaction A-B and neglect the interaction B-C because the concentration of substitutional atoms B and the concentration of interstitial atoms C are small. The potential parameters D, r_0, m, n are given in Table 1. Considering the interaction between Au and Si and between Au and Cu, we use the following approximation

$$\varphi_{A-X} \approx \frac{1}{2} (\varphi_{A-A} + \varphi_{X-X}) \quad (X = B, C).$$

Table 1. The parameters D, r_0, m, n of the Mie-Lennard-Jones potential [18, 19]

Interaction	m	n	$D/k_B\sigma$	$r_0(10^{-10}\text{m})$
Si-Si [18]	6	12	32701.7	2.295
Au-Au [19]	1.96	15.56	7411.5	2.8751
Cu-Cu [19]	3.03	8.37	6841.3	2.5487

SMM calculations for nonlinear deformation of Au, AuSi are summarised in tables from Table 2 to Table 4 and illustrated in figures from Figure 1 to Figure 4. At $P = 0$, we choose the value of experimental stress $\sigma_{0.2\%}$ for Au and AuSi according to each temperature from the experimental results of Chang and Himmel (1966) [20] by the formula $\sigma_{0.2\%} = E \cdot \varepsilon_{0.2\%}$. The graph $f(\varepsilon)$ always exits $\varepsilon = \varepsilon_F$ so that $f = f_{\max}$. Specifically when $c_{Si} = 0$ then $\varepsilon_F = 9.7\%$ corresponding to $f_{\max} = 24.69$ GPa. When $c_{Si} = 1\%$ then $\varepsilon_F = 9.7\%$ corresponding to $f_{\max} = 22.91$ GPa. From that, we calculate the values of the maximum real stress $\sigma_{1\max}$ and the elastic deformation limit σ_e corresponding to the strain ε_e . The graphs of $f(\varepsilon)$ and $\sigma_1(\varepsilon)$ for Au and AuSi are described in figures from Figure 1 to Figure 3, where we compare SMM calculations with experiments of Khatibi *et al.* (2018) [21]. Numerical calculations are summarised in Table 2 và Table 3.

According to SMM calculations for Au at $P = 0$ and $T = 300$ K when $\varepsilon_F = 9.7\%$ then $\sigma_1 = \sigma_{1\max}$ and when $\varepsilon_e = 0.16\%$ then $\sigma_1 = \sigma_e$. Figure 1 describes the real stress – strain $\sigma_1(\varepsilon)$ of Au at $T = 300$ K and $P = 0$, where the SMM calculations are compared with experiments of Khatibi *et al.* (2018) [21]. When the strain ε is in the range from zero to near 4%, the SMM calculations are in very good agreement with experiments [21] (the error of maximum real stress is 0.6%).

Table 2. ε_F corresponding to f_{\max} , $\sigma_{1\max}$ and σ_e corresponding to ε_e (%) for AuSi at $T = 300$ K and $P = 0$ calculated by SMM and from EXPT of Khatibi *et al.* (2018) [21]

c_{Si} (%)	Method	$\sigma_{1\max}$ (MPa)	ε_F (%)	σ_e (MPa)	ε_e (%)
0	SMM	207.85	9.7	158.48	0.16
0	EXPT [21]	209.00	3.5	130.00	-
1	SMM	205.75	9.7	158.35	0.18
2	SMM	203.92	9.7	158.43	0.20

Table 3. $\varepsilon_F(T, c_{Si})$ corresponding to f_{\max} and $\sigma_e(T, c_{Si})$ corresponding to $\varepsilon_e(T, c_{Si})$ for AuSi at $P = 0$

T (K)	c_{Si} (%)	$\sigma_{1\max}$ (MPa)	ε_F (%)	σ_e (MPa)	ε_e (%)
500	0	207.10	7.9	170.15	0.20
	1	190.11	7.9	156.48	0.20
	2	174.32	7.9	143.74	0.21
800	0	199.11	6.0	176.43	0.27
	1	185.52	6.0	164.78	0.28
	2	167.07	6.0	148.48	0.29

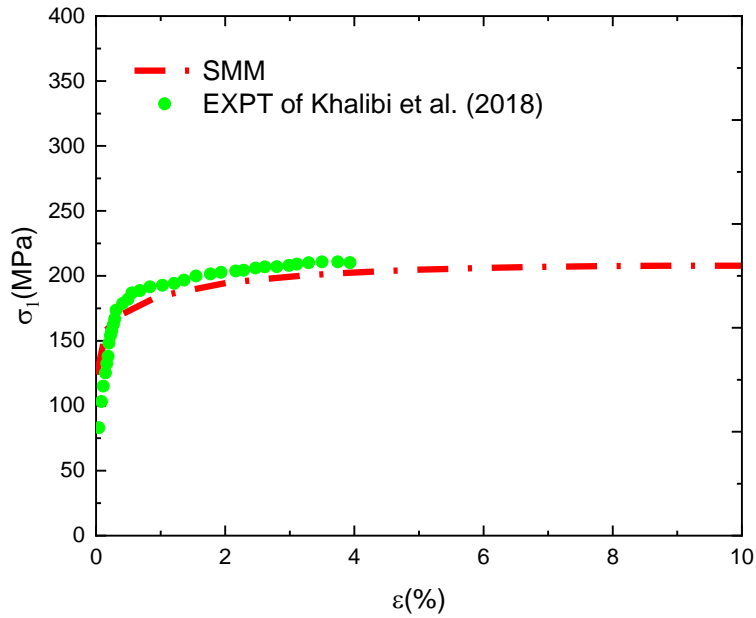


Figure 1. $\sigma_1(\varepsilon)$ of Au at $T = 300$ K and $P = 0$ calculated by SMM from EXPT of Khatibi et al. (2018) [21]

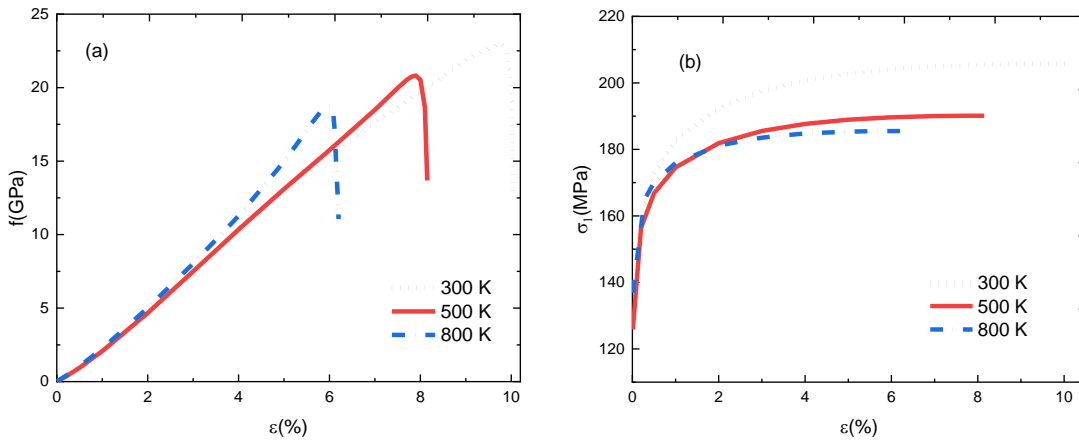


Figure 2. (a) $f(\varepsilon, T)$ and (b) $\sigma_1(\varepsilon, T)$ for AuSi at $c_{Si} = 1\%$ and $P = 0$ calculated by SMM

When considering the nonlinear deformation of AuSi with respect to pressure, the values of experimental stress $\sigma_{0.2\%}$ of AuSi at $T = 300$ K, pressures $P = 2.55$ GPa, 4.88 GPa, 9.47 GPa, and 18.78 GPa are chosen according to experiments of Yoneda *et al.* (2017) [22]. Figure 4 describes the dependence of the deformation energy density and the real stress on strain and pressure for AuSi.

According to tables from Table 2 to Table 4 for AuSi at the same temperature and pressure when the interstitial atom concentration increases, the maximum real stress σ_{1max} and the limit of elastic deformation σ_e slightly decrease. For example for AuSi at $P = 0$ and $T = 300$ K when the interstitial atom concentration c_{Si} tăng từ 0 đến 2%, σ_{1max} decreases from 207.85 to 203.92 MPa (down 1.89%) and σ_e decreases from 158.48 to 158.43 MPa (down 0.03%).

Table 4. $\varepsilon_F(P, c_{Si})$ corresponding to f_{max} , $\sigma_{1max}(P, c_{Si})$ and $\sigma_e(P, c_{Si})$ corresponding to $\varepsilon_e(P, c_{Si})$ for AuSi at $T = 300$ K

P (GPa)	c_{Si} (%)	σ_{1max} (MPa)	ε_F (%)	σ_e (MPa)	ε_e (%)
2.55	0	253.23	10.1	192.29	0.18
	1	235.26	10.1	179.24	0.19
	2	218.47	10.1	167.02	0.19
4.88	0	324.48	10.4	248.07	0.22
	1	301.66	10.4	231.43	0.22
	2	280.45	10.4	215.95	0.23
9.47	0	373.12	10.9	280.66	0.21
	1	347.16	10.9	262.10	0.22
	2	322.98	10.9	244.76	0.23
18.78	0	597.41	11.8	448.39	0.28
	1	555.91	11.8	418.90	0.29
	2	517.47	11.8	391.52	0.30

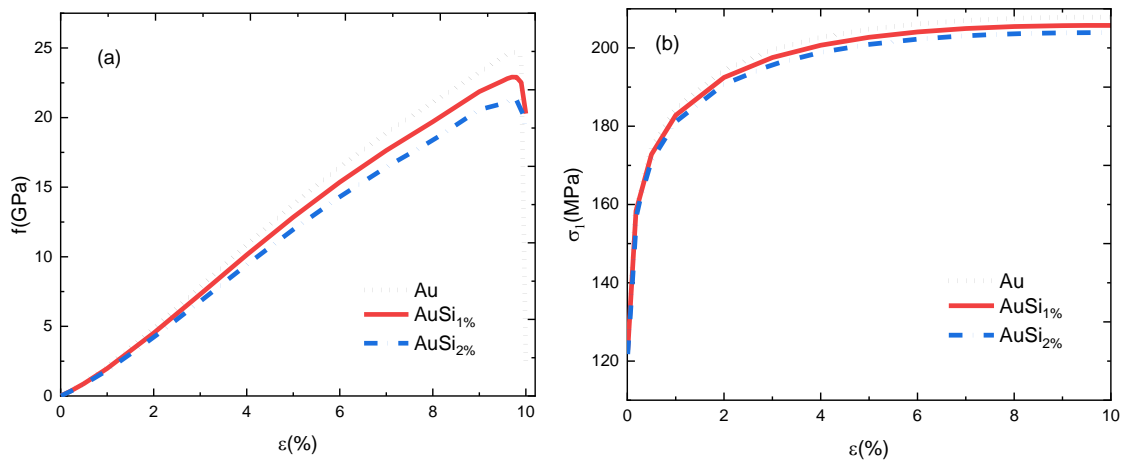


Figure 3. (a) $f(\varepsilon, c_{Si})$ and (b) $\sigma_1(\varepsilon, c_{Si})$ for AuSi at $T = 300$ K and $P = 0$ calculated by SMM

For Au and AuSi at the same pressure and interstitial atom concentration when temperature increases, $\sigma_{1\max}$ and σ_e decrease. For example for AuSi at $P = 0$ and $c_{Si} = 2\%$ when temperature increases from 300 to 800 K, $\sigma_{1\max}$ decreases from 203.92 to 167.07 MPa (down 18.07%) and σ_e decreases from 158.43 to 148.48 MPa (down 6.28%). This rule is consistent with the SMM calculations of Hoa (2007) [23] for metals and substitutional alloys.

For Au and AuSi at the same temperature and interstitial atom concentration when pressure increases, $\sigma_{1\max}$ and σ_e strongly increases. For example for AuSi at $T = 300$ K and $c_{Si} = 1\%$ when pressure increases from 2.55 to 18.78 GPa, $\sigma_{1\max}$ increases from 235.26 to 555.91 MPa (up 136.30%) and σ_e increases from 179.24 to 418.90 MPa (up 133.71%).

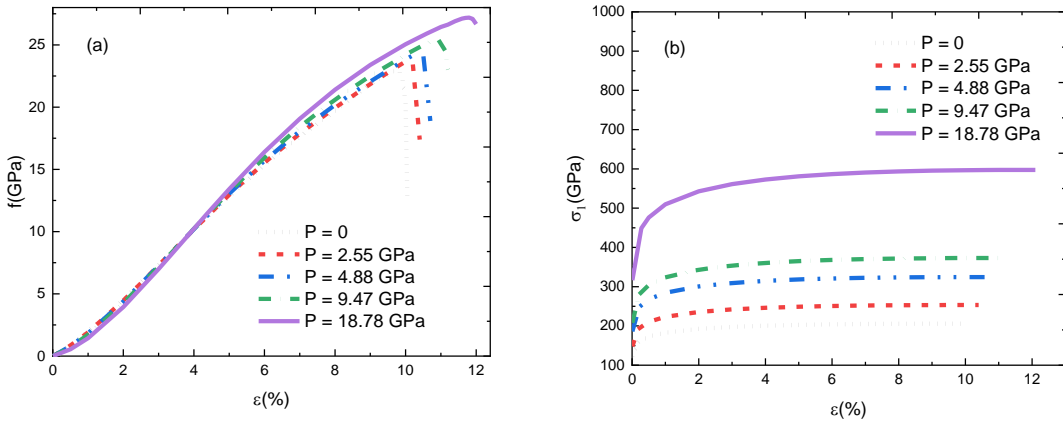


Figure 4. (a) $f(\epsilon, P)$ and (b) $\sigma_1(\epsilon, P)$ for AuSi at $c_{Si} = 2\%$ and $T = 300$ K calculated by SMM

SMM calculations for nonlinear deformation of Au, AuSi are summarised in tables from Table 5 to Table 7 and illustrated in figures from Figure 5 to Figure 8.

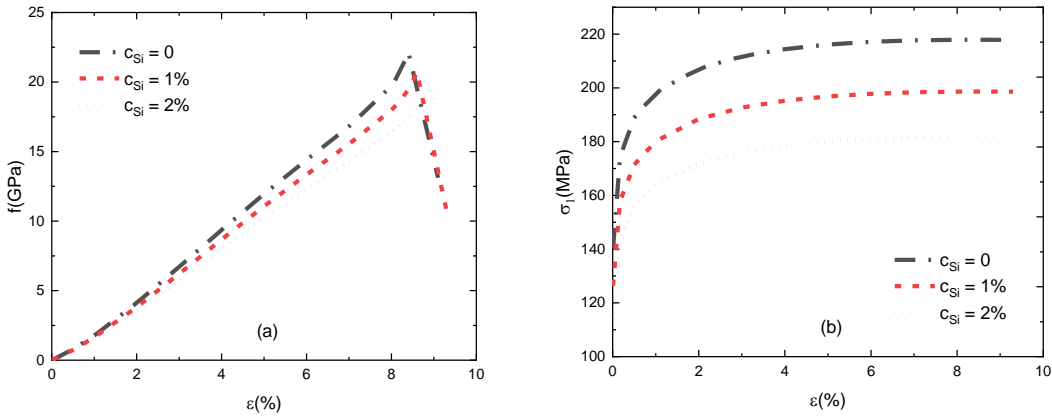


Figure 5. (a) $f(\epsilon, c_{Si})$ and (b) $\sigma_1(\epsilon, c_{Si})$ for AuCuSi at $c_{Cu} = 10\%$, $T = 300$ K and $P = 0$

Table 5. $\varepsilon_F(c_{Si}, T)$ corresponding to $f_{\max}(c_{Si}, T)$, $\sigma_{1\max}(c_{Si}, T)$ and $\sigma_e(c_{Si}, T)$ corresponding to $\varepsilon_e(c_{Si}, T)$ for AuCuSi at $c_{Cu} = 10\%$ and $P = 0$

$T(K)$	$c_{Si} (%)$	$\varepsilon_F (%)$	$\sigma_{1\max} (MPa)$	$\varepsilon_e (%)$	$\sigma_e (MPa)$
300	0	8.4	217.91	0.17	174.67
	1	8.6	198.64	0.17	158.13
	2	8.9	181.89	0.17	143.34
500	0	7.1	219.56	0.21	187.74
	1	7.3	184.33	0.19	154.43
	2	7.6	174.56	0.20	144.84
700	0	5.8	184.14	0.21	162.16
	1	6.3	160.71	0.20	139.42
	2	6.5	148.26	0.20	127.51
800	0	5.2	174.63	0.22	156.94
	1	5.6	157.59	0.22	139.89
	2	5.9	142.29	0.22	125.11

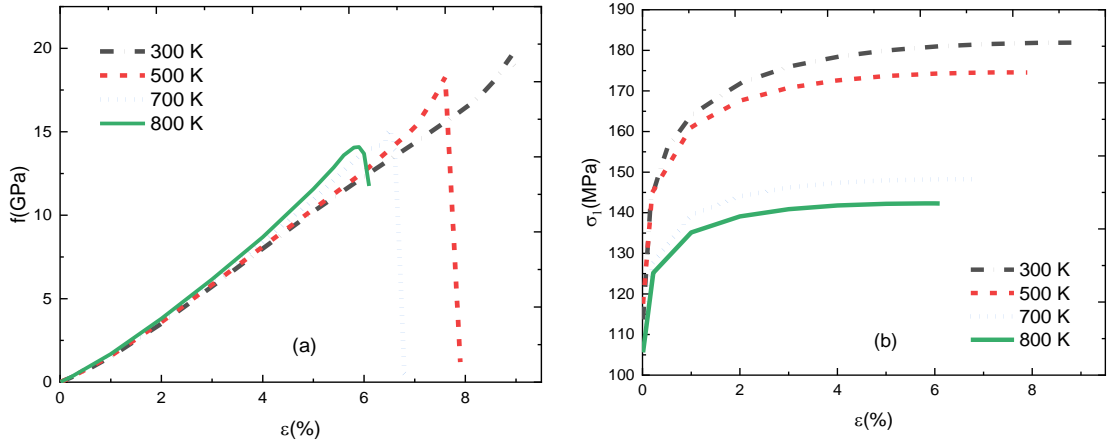


Figure 6. (a) $f(\varepsilon, T)$ and (b) $\sigma_1(\varepsilon, T)$ for AuCuSi at $c_{Cu} = 10\%$, $c_{Si} = 2\%$ and $P = 0$

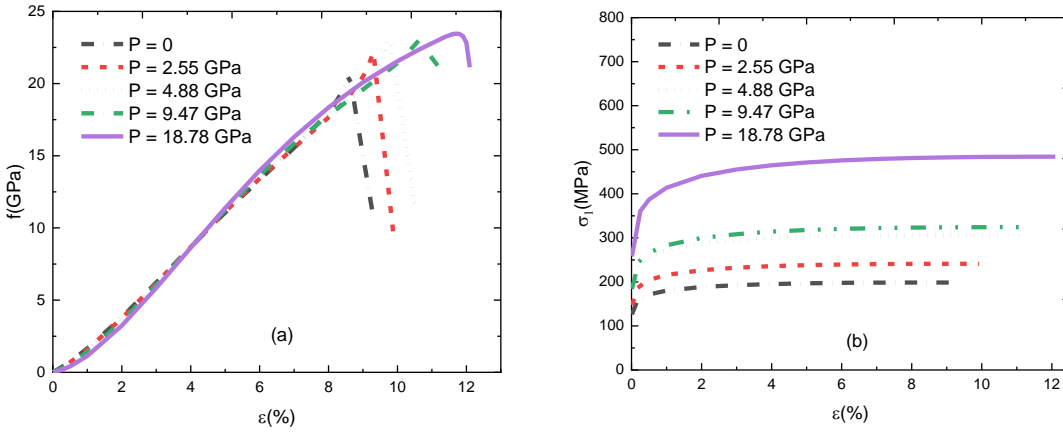


Figure 7. (a) $f(\varepsilon, P)$ and (b) $\sigma_1(\varepsilon, P)$ for AuCuSi at $c_{Cu} = 10\%$, $c_{Si} = 1\%$ and $T = 300$ K

Table 6. $\varepsilon_F(P, c_{Si})$ corresponding to $f_{max}(P, c_{Si})$, $\sigma_{1max}(P, c_{Si})$ and $\sigma_e(P, c_{Si})$ corresponding to $\varepsilon_e(P, c_{Si})$ for AuCuSi at $c_{Cu} = 10\%$ and $T = 300$ K

P (GPa)	c_{Si} (%)	ε_F (%)	σ_{1max} (MPa)	ε_e (%)	σ_e (MPa)
0	0	8.4	217.91	0.17	174.67
	1	8.6	198.64	0.17	158.13
	2	8.9	181.89	0.17	143.34
2.55	0	9.0	264.42	0.19	209.44
	1	9.3	241.07	0.19	188.99
	2	9.4	218.74	0.19	170.84
4.88	0	9.5	333.63	0.23	263.56
	1	9.7	306.75	0.23	240.95
	2	9.7	269.01	0.22	210.59
9.47	0	10.5	376.35	0.22	287.19
	1	10.6	324.28	0.21	245.25
	2	11.0	282.83	0.19	209.92
18.78	0	11.8	530.56	0.24	392.89
	1	11.7	484.18	0.25	360.00
	2	11.7	442.08	0.25	328.88

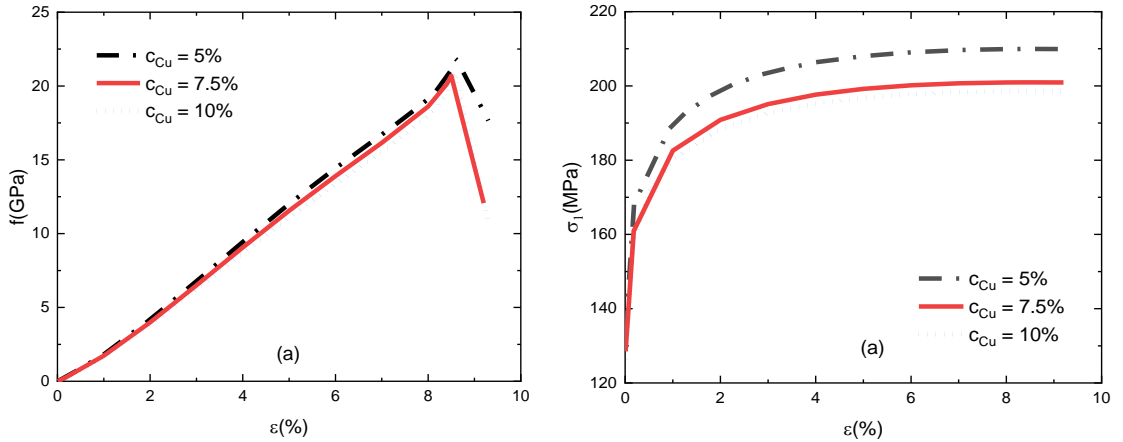


Figure 8. (a) $f(\varepsilon, c_{Cu})$ and (b) $\sigma_1(\varepsilon, c_{Cu})$ for AuCuSi at $c_{Si} = 1\%$, $T = 300\text{ K}$ and $P = 0$

Table 7. $\varepsilon_F(P, c_{Cu})$ corresponding to $f_{\max}(P, c_{Cu})$, $\sigma_{1\max}(P, c_{Cu})$ and $\sigma_e(P, c_{Cu})$ corresponding to $\varepsilon_e(P, c_{Cu})$ for AuCuSi at $c_{Si} = 1\%$ and $T = 300\text{ K}$

$P(\text{GPa})$	$c_{Cu} (\%)$	$\varepsilon_F (\%)$	$\sigma_{1\max} (\text{MPa})$	$\sigma_e (\text{MPa})$	$\varepsilon_e (\%)$
0	5	8.6	209.96	0.19	168.13
	7.5	8.5	200.92	0.18	160.81
	10	8.6	198.64	0.17	158.13
2.55	5	9.3	255.95	0.21	201.98
	7.5	9.3	250.19	0.20	196.92
	10	9.3	241.07	0.19	188.99
4.88	5	9.7	323.48	0.24	255.63
	7.5	9.8	314.46	0.23	246.88
	10	9.7	306.75	0.23	240.95
9.47	5	11.0	364.39	0.23	275.33
	7.5	11.1	355.69	0.22	267.00
	10	10.6	324.28	0.21	245.25
18.78	5	11.8	522.18	0.27	390.48
	7.5	11.7	506.47	0.26	378.61
	10	11.7	484.18	0.25	360.00

According to tables from Table 5 to Table 7 and figures from Figure 5 to Figure 8 for AuCuSi at the same temperature and pressure when the interstitial atom concentration increases, the maximum real stress $\sigma_{1\max}$ and the limit of elastic deformation σ_e decrease.

For example for AuSi at $T = 300$ K, $P = 2.55$ GPa, 300 K $c_{Cu} = 10\%$ when c_{Si} increases from 0 to 2%, σ_{1max} decreases from 264.42 to 218.74 MPa (down 17.27%) and σ_e decreases from 209.44 to 170.84 MPa (down 18.43%).

For AuCuSi at the same temperature, pressure, and interstitial atom concentration when the substitutional atom concentration increases, σ_{1max} and σ_e decrease. For example for AuCuSi at $T = 300$ K, $P = 0$ and $c_{Si} = 1\%$ when c_{Cu} increases from 5 to 10%, then σ_{1max} decreases from 209.96 to 198.64 MPa (down 5.39%) and σ_e decreases from 168.13 to 158.13 MPa (down 5.7%).

For AuCuSi at the same pressure, interstitial atom concentration and substitutional atom concentration when temperature increases, then σ_{1max} and σ_e decrease. For example for AuCuSi at $P = 0$, $c_{Cu} = 10\%$ and $c_{Si} = 2\%$ when temperature increases from 300 to 800 K, then σ_{1max} decreases from 181.89 to 142.29 MPa (down 21.77%) and σ_e decreases from 143.34 to 125.11 MPa (down 12.72%).

For AuCuSi at the same temperature, interstitial atom concentration and substitutional atom concentration when pressure increases, then σ_{1max} and σ_e strongly increase. For example for AuCuSi at $T = 300$ K, $c_{Si} = 2\%$ and $c_{Cu} = 10\%$ when pressure increases from zero to 18.78 GPa, then σ_{1max} increases from 198.64 to 484.18 MPa (up 143.75%) and σ_e increases from 143.34 to 328.88 MPa (up 129.44%).

3. Conclusions

On the basis of the model and the theory of nonlinear deformation for FCC substitutional and interstitial ternary alloy built by the statistical moment method, we perform numerical calculations for Au, AuSi, and AuCuSi in the temperature range from 300 to 800 K, in the pressure range from zero to 18.78 GPa, in the range of interstitial atom concentration from zero to 2% and in the range of substitutional atom concentration from 5 to 10%. When the strain ε is in the range from zero to near 4%, the SMM calculations for the real stress-strain $\sigma_1(\varepsilon)$ of Au at $T = 300$ K and $P = 0$ are in very good agreement with experiments [21] (the error of maximum real stress is 0.6%). The maximum real stress and the elastic strain limit of FCC substitutional and interstitial ternary alloy decrease as the interstitial atom concentration increases. This rule is similar to that of FCC binary interstitial alloy. The nonlinear deformation quantities of FCC substitutional and interstitial ternary alloy both decrease with increasing temperature and increase with increasing pressure. This rule is similar to that of FCC interstitial binary alloy and that of FCC main metal. The nonlinear deformation quantities of FCC substitutional and interstitial ternary alloy all change slowly with the substitution atom concentration. This rule is similar to that of FCC substitutional binary alloy. When the interstitial and substituted atom concentrations are zero, the stress-strain curve obtained by SMM agrees well with experiments. Numerical results without comparative data are new results and are a reference source for prediction and experimental orientation in the future.

REFERENCES

- [1] Nyilas R.D., Kobas M., and Spolenak R., 2009. Synchrotron X-ray microdiffraction reveals rotational plastic deformation mechanisms in polycrystalline thin films. *Acta Materialia*, Vol. 57, Iss.13, pp.3738-3753.
- [2] Chariotis I., Bateson C., Timpano K., McCarty A.S., Barker N.S., and Stanec J.R., 2007. Strain rate effects on the mechanical behavior of nanocrystalline Au films. *Thin Solid Films*, Vol. 515, Iss. 6, pp. 3183-3189.
- [3] https://structx.com/Material_Properties_0003a.html.
- [4] <https://www.azom.com/proprerties.aspx?Arrticla ID=600>.
- [5] Mehl M.J., Papacostantopoulos D.A., 1996. Applications of a tight-binding total-energy method for transition and noble metals: elastic constants, vacancies and surfaces of monatomic metals. *Physical Review B*, Vol. 54, Iss. 7, p. 4519.
- [6] Esfahani M.N., and Jabbari M., 2020. Molecular Dynamics Simulations of deformation mechanisms in the mechanical response of nanoporous gold. *Materials*, Vol. 13, No. 9, p. 2071.
- [7] Tang N. and Hung V.V., 1988. Investigation of the thermodynamic properties of anharmonic crystals by the momentum method, I. General results for face-centered cubic crystals. *Physica Status Solidi (b)*, Vol. 149, Iss. 2, pp. 511-519.
- [8] Tang N. and Hung V. V., 1990. Investigation of the thermodynamic properties of anharmonic crystals by the momentum method, III. Thermodynamic properties of the crystals at various pressures. *Physica Status Solidi (b)*, Vol. 162, No. 2, pp. 371-377.
- [9] Hung V. V., 2009. *Statistical moment method in studying elastic and thermodynamic properties of crystals*, University of Education Publishing House.
- [10] Hoc N. Q., Tinh B. D., Cuong T. D. and Viet L. H., 2019. Study on the melting of defective interstitial alloys TaSi and WSi with BCC structure. *Journal of the Korean Physical Society*, Vol. 71, Iss. 8, pp. 801-805.
- [11] Tuyen L. T. C., Hoc N. Q., Tinh B. D., Cuong T. D. and Vinh D. Q., 2019. Study on the melting of interstitial alloys FeH and FeC with BCC structure under pressure. *Chinese Journal of Physics*, Vol. 59, pp. 1-9.
- [12] Tuyen L. T. C., Hoc N. Q., Tinh B. D., Hanh P. T. M., Cuong T. D. and Viet L. H., 2019. Thermal expansion coefficient of BCC defective substitutional alloy AB with interstitial atom C. *Modern Physical Letter B*, Vol. 33, Iss. 13, ID 1950165.
- [13] Hoa N.T., Hoc N.Q., Coman G., Cuong T.D. and Viet L.H., 2019. Thermodynamic property of FCC interstitial alloy with defects, *Proc. of the 8th International Conference on Material Science and Engineering (UGALMAT 2018)*, 11-13 October 2018. "Dunarea de Jos" University of Galati, Romania, *IOP Conference Series: Materials Science and Engineering*, Vol. 385, ID 012018.
- [14] Hoc N.Q., Tinh B.D., Tuan L.D. and Hien N.D., 2016. Elastic deformation of binary and ternary interstitial alloys with FCC structure and zero pressure: Dependence on temperature, concentration of substitution atoms and concentration of interstitial atoms. *HNUE Journal of Science, Mathematical and Physical Sciences*, Vol. 61, Iss. 7, pp.47-57.

- [15] Hoc N.Q., Hien N.D. and Thang D.Q., 2018. Elastic deformation of alloy AuSi with FCC structure under pressure. *HNUE Journal of Science, Natural Sciences*, Vol. 63, Iss. 6, pp.74-83.
- [16] Hoc N. Q., Tinh B. D., Coman G. and Hien N. D., 2020. On the melting of alloys FeX (X = Ni, Ta, Nb, Cr) under pressure up to 5 Gpa. *Journal of the Physical Society of Japan*, Vol. 89, Iss.11, ID 114602.
- [17] Hoc N.Q., Hoa N.T. and Hien N.D., 2019. Build the theory of nonlinear deformation for BCC and FCC substitutional alloys AB with interstitial atom C under pressure. *HNUE Journal of Science, Natural Sciences*, Vol. 64, Iss. 6, pp. 45-56.
- [18] Magomedov M.N., 1987. On calculating the Debye temperature and the Gruneisen parameter. *Journal of Physical Chemistry*, Vol. 61, Iss. 4, pp. 1003-1009 (in Russian).
- [19] Magomedov M.N., 2006. The calculation of the parameters of the Mie-Lennard-Jones potential. *High Temperature*, Vol. 44, Iss. 4, pp. 513-529.
- [20] Chang Y.A. and Himmel L., 1966. Temperature dependence of the elastic constants of Cu, Ag, and Au above room Temperature. *Journal of Applied Physics*, Vol. 37, Iss. 9, pp. 3567-3572.
- [21] Khatibi G., Mazloum-Nejadari A., Lederer M., Delshadmanesh M. and Czerny B., 2018. Fatigue lifetime modeling of Cu and Au fine wires. *MATEC Web Conference*, Vol. 165, ID 06002.
- [22] Yoneda A., Fukui H., Gomi H., Kamada S., Xie L. and Hirao N., 2017. Single-crystal elasticity of gold up to ~20 GPa: Bulk modulus anomaly and implication for a primary pressure scale. *Japanese Journal of Applied Physics*, Vol. 56, ID 095801.
- [23] Hoa N.T., 2007. *Study on elastic - nonlinear deformation and elastic wave propagation process of metals, alloys by statistical moment method*. Ph.D. Thesis, Hanoi National University of Education.